Atomic and molecular effects on angular distributions of photoelectrons scattered from surfaces

1996 J. Phys.: Condens. Matter 8 2305

(http://iopscience.iop.org/0953-8984/8/14/007)

J. Phys.: Condens. Matter **8** (1996) 2305–2316. Printed in the UK

Atomic and molecular effects on angular distributions of photoelectrons scattered from surfaces

A A Pavlychev and N G Fominykh

Institute of Physics, St Petersburg University, St Petersburg, 198904, Russian Federation

Received 18 October 1995

Abstract. The quasiatomic approach is applied for the first time to the consideration and computation of angular distributions of (x-ray) photoelectrons scattered from surfaces. The anisotropic region surrounding an ionized-core atom in a specimen is regarded as acting as an electron-optical lens focusing or defocusing the initial (prescattering) photoelectron flux along various directions. The quasiatomic equations describing the photoelectron angular distributions as functions of the electron-optical properties of the surroundings are obtained, and stereographic projections of the photoelectron yield from model octahedral clusters (such as $[SiF_6]$, $[Na^+F_6^-]$ and $[F^-Na_6^+]$) are computed with their help. Calculations of the low- and medium-energy photoelectron diffraction patterns show that the splitting of atomic $[\mathrm{core}^{-1}El]$ transitions and the ll'-hybridization of the atomic continuous states dominate the focusing effect. It is revealed that: (1) a central role is played by the collective action of all of the atoms in the environment, whose symmetry compels the major directions of photoelectron yield to coincide with fourfold and threefold rotation axes rather than with directions to the nearest neighbours; (2) the low- and medium-energy diffraction patterns are highly sensitive to the electronic structure of the ionized atom and the integral electron-optical properties of the surroundings; and (3) the photoelectron angular distributions change dramatically when resonant inner-shell photoemission is achieved, and correlate with the symmetry of the highly excited molecular orbitals. The relationship between the description in terms of quasiatomic waves and that in terms of multiply scattered waves is discussed.

1. Introduction and general remarks

Angular distributions of Auger electrons and (x-ray) photoelectrons are widely applied in the determination and modelling of the atomic geometry of surfaces [1–6]. Due to the strong localization of x-ray absorption in polyatomic systems, it is the symmetry of the surroundings of the excited-core atom (g) that generally determines the angular dependence of the photoelectron yield $J(\Omega)$. For high kinetic energies E of ejected electrons (usually $E > 500$ eV) the complex diffraction pattern is simplified—as a strong forward-scattering of the electrons by nearest-neighbour atoms in the vicinity of the emitter gives rise to characteristic maxima of $\boldsymbol{J}$ along close-packed low-index directions in a specimen [1, 2].

The sensitivity of photoelectron diffraction to the geometry and the atomic composition of the surface is dramatically enhanced in low- and medium-energy regimes [1, 7, 8]. For these energies, the simple mechanism no longer applies, because the basic approximations—such as (i) using plane waves to represent outgoing electrons and (ii) assuming that the electron density distributions of the surrounding atoms that dominate over the forward-scattering amplitudes in the formation of the diffraction pattern are spherically symmetrical—become invalid. The orbital momentum l of initial (prescattering) outgoing

0953-8984/96/142305+12$19.50

electronic waves and the angular deformations of the electron density distributions of the emitters and the scatterers cannot be ignored.

The l-dependence of the pattern originates from the inner-shell atomic photoeffect and characterizes the electronic structure of the emitter. Its importance was demonstrated experimentally in [7]. The dynamical (multiscattering) effects reinforce the role of nonspherical deformation of atoms in the assembly of those atoms, and the role of its symmetry in the formation of the diffraction pattern. Local multipole momenta (μ) of the potential of the surroundings characterize these atomic deformations which, in their turn, can be connected with surface chemical bonding effects such as interatomic electronic *charge transfer, splitting* and *hybridization* of atomic states, and *localization* (orientation) of chemical bonds.

To study these chemical effects on photoelectron diffraction, accurate definitions of the chemical states of an atom in a polyatomic system and, especially, its highly excited states are required. That is why it is of particular value to have a clear physical model, allowing one to highlight the main relationships between low-energy photoelectron angular distributions and chemical bonding. To reveal these we primarily need to connect $J(\Omega)$-dependences with *atomic* characteristics of emitters and scatterers and with the molecular structure of the compound under study. The multiply-scattered-waves (MSW) method lying at the heart of Auger and photoelectron diffraction descriptions [9–11] encounters insuperable difficulties because of the use of the muffin-tin (MT) approximation [12], making it impossible to obtain a correct definition of the atomic chemical states in compounds using this method.

In the present work, for the first time the quasiatomic (QA) approach [13–15] is applied in the study of the atomic and molecular effects on photoelectron angular distributions and in computing them for various octahedral clusters, with the help of QA equations. Earlier, the QA approach was successfully used in descriptions of the spectral dependence of the inner-shell photoionization and x-ray absorption of various chemical compounds [13–15]. In that early work, the central role of radial and angular deformations in the formation of atomic highly excited and ionized states was revealed, and the fact that this conclusion does not militate against the main results obtained in the framework of the MSW approach was discussed. Hence one can consider an alternative interpretation of inner-shell photoprocesses.

2. QA treatment

In the framework of the QA model, inner-shell photoionization is regarded as a process occurring in an atom (g) incorporated into its surroundings. The initial atomic parameters of this process are modified by the impact of the surroundings, described by means of the relevant electron-optical characteristics, such as the reflectivity, transmission, index of refraction and energy-loss function. On the supposition that the x-ray radiation is unpolarized and that the effects of the partially filled orbitals of the ionized-core atom in the compounds under study are negligible, the anisotropy of the electron-optical characteristics of the surroundings must be the cause of the appearance of the angular distribution of the initially isotropic atomic photoelectron flux. This means that the surroundings act as an anisotropic electron-optical lens, and focus and/or defocus the atomic photoelectron fluxes along various directions Ω_S. Since an anisotropic environment (i) splits degenerate atomic [core^{-1}El] excitations into a series of [core$^{-1}El\Gamma$] ones (where Γ is an irreducible representation of the symmetry point group $\mathcal{G}$ of atom g in the compound) and (ii) mixes l-harmonics with l'-harmonics ($l \neq l'$) in the excited-core atom [9], these effects are regarded as being responsible for the changes of angular distribution of the photoelectrons that are knocked

out of position and for the anisotropy of their yield. If the interaction between partially filled atomic orbitals is important, the initial anisotropy must be taken into consideration in describing the $J(\Omega)$-distribution of the surroundings. In this work the features caused by this interaction are not studied or discussed.

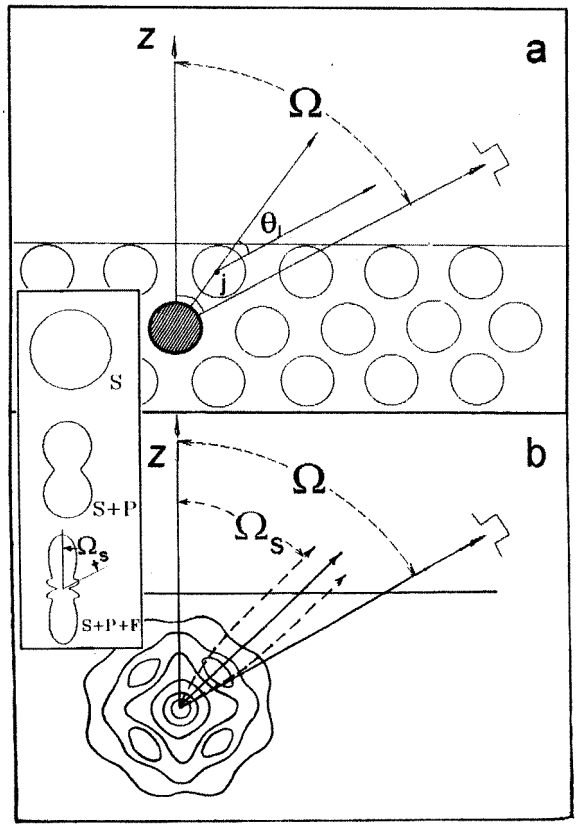

Figure 1. The schemes illustrating the description of the angular distributions of photoelectrons scattered from surfaces in the framework of the MSW (a) and the QA (b) approaches are shown. θ_j is a scattering angle for scattering by environment atom j. Ω_j and Ω characterize directions along the crystallographic axis and towards a detector respectively. (b) The photoelectron paths are stretched along directions with high electron-optical density. Inset: various angular distributions of $Y_{lm}(\Omega)$-harmonics; their combination reproduces the angular distribution of atomic photoelectrons due to the impact of the surroundings.

Two schemes illustrating the QA and MSW descriptions of $J(\Omega)$-formation are shown in figure 1. Instead of describing the scattering of photoelectrons by each single environment atom, j (as is usually done in the MSW method), we consider their propagation through the assembly of atoms taken together. The scattering amplitudes $f(\vartheta_j)$ for scattering by neighbouring atoms (the scattering angles ϑ_j shown in figure 1(a) are defined in the frame centred at environment atom j) are not used for the characterization of $J(\Omega)$-features; these are now simulated by sets of symmetry-adapted $l'\Gamma$-harmonics with the relevant angular parts $Y_{l'\Gamma}(\Omega)$. The inset in figure 1 shows how an angular distribution can be reproduced with the help of the $Y_{l'\Gamma}(\Omega)$-functions. Their dependence on $\mathcal{G}$ makes clear the connection between Ω_S and the crystallographic directions in a specimen. The photoelectron kinetic

energy E plays a very important role in determining the number of l'-harmonics. Its maximal value, rising with E, can be estimated as $n_{l'_{max}} = kR$, where $E = k^2$ and R is the radius of the scattering region.

The localized orbital method [16, 17] and the variable-phase approach [18, 19] lie at the heart of the QA description of inner-shell photo-processes in polyatomics [13–15]. Localized-atom-like $\varphi_g(E, \boldsymbol{r})$-functions are presented as superpositions of electronic waves incoming to and outgoing from atom g: $A^-_{ll'\Gamma t}\varphi^-_{l'}(r)Y_{l'\Gamma\gamma t}(\Omega)$ and $A^+_{ll'\Gamma t}\varphi^+_{l'}(r)Y_{l'\Gamma\gamma t}(\Omega)$, respectively, where $Y_{l'\Gamma t}(\Omega)$ is a symmetry-adapted spherical function in the coordinate frame centred at atom g, l and l' are the orbital momenta of the photoelectrons before and after their interaction with the surroundings, and the subscripts γ and t enumerate functions referring to a degenerate Γ representation and equivalent representations with the given l-value [20] respectively. (Hereafter the subscripts γ and t are omitted, assuming summation over them). The $A^{\pm}_{ll'\Gamma t}$-coefficients are determined as a result of multiple reflections of photoelectrons and their scattering by atom g.

At large distances beyond the sphere of radius R_g, the amplitude of the reflected waves is negligible and the $\varphi_g(E, \boldsymbol{r})$-function can be written as

$$\varphi_g(E,\boldsymbol{r}) = \sum_{l'\Gamma}\left[\mathbf{T} + \mathbf{BST} + \ldots + (\mathbf{BS})^n\mathbf{T}\right]_{ll'\Gamma}\varphi^+_{l'}(r)Y_{l'\Gamma}(\Omega)$$
$$\sim \sum_{l'\Gamma}\left[\frac{\mathbf{T}}{\mathbf{1}-\mathbf{BS}}\right]_{ll'\Gamma}\frac{1}{r}\exp\left[\mathrm{i}\left(kr - \frac{l'\pi}{2}\right)\right]Y_{l'\Gamma}(\Omega). \tag{1}$$

Here $\mathbf{S}$ is a diagonal scattering matrix whose nonzero elements are equal to $\exp(2\mathrm{i}\delta_l)$, and $\mathbf{B} = \{B_{ll'\Gamma}\}$ and $\mathbf{T} = \{T_{ll'\Gamma}\}$ are the matrices describing the reflection and transmission through the surroundings. Using equation (1) a full dynamical (i.e. multiple-scattering) description of the photoelectron flux $\boldsymbol{J} = \varphi_g\boldsymbol{\nabla}\varphi^*_g - \varphi^*_g\boldsymbol{\nabla}\varphi_g$ emitted from atom g and having gone through the surroundings (i.e. for $r > R_g$) is provided.

The matrices $\mathbf{B}(E, \boldsymbol{r})$ and $\mathbf{T}(E, \boldsymbol{r})$ are computed by solving the nonlinear first-order (Riccaty-type) differential equations [13, 21]:

$$\frac{\mathrm{d}\mathbf{B}}{\mathrm{d}r} = [\mathbf{\Phi}^+ + \mathbf{B}\mathbf{\Phi}^-]\mathcal{W}[\mathbf{\Phi}^+ + \mathbf{\Phi}^-\mathbf{B}] \tag{2}$$

$$\frac{\mathrm{d}\mathbf{T}}{\mathrm{d}r} = -\mathbf{\Phi}^-\mathcal{W}[\mathbf{\Phi}^+ + \mathbf{\Phi}^-\mathbf{B}]\mathbf{T} \tag{3}$$

respectively, with the boundary conditions

$$\mathbf{B}(R_g) = 0 \qquad \mathbf{T}(b) = \{\delta_{ll'}\}. \tag{4}$$

The second condition shows that had the potential of the surroundings been ignored, the outgoing photoelectron waves would have appeared in two (or one) dipole-allowed channels with $l = l_0 \pm 1$ only. All other harmonics with $l' \neq l$ in the sum (1) appear as a result of series of reflections and transmissions of initially isotropic El-waves through the anisotropic surroundings. $\mathcal{W}$ is the potential of the surroundings (the pseudopotential):

$$\mathcal{W} = \sum_{\mu\geqslant 0} W_\mu(r)Y_\mu(\Omega) \tag{5}$$

where W_μ is the 2^μ-pole momentum of the environment atom pseudopotential superposition

$$\sum_{j\neq g} v^{ps}(\boldsymbol{r} - \boldsymbol{R}_j).$$

The diagonal matrices $\mathbf{\Phi}^\pm$ are formed from the atomic $\varphi^\pm_{gl\Gamma}$-functions with asymptotes

$$\exp[\pm\mathrm{i}(kr - l\pi/2 + \text{Coulombic phase})]$$

centred at ionized-core atoms. Since the photoelectron $\varphi_g(E, \boldsymbol{r})$-function is considered over all of coordinate space as a sum over partial states centred at atom g, their mixing induced by the anisotropy of the surroundings can be attributed to the effect of hybridization of atomic continuum states in a polyatomic system.

The angular dependence of the photoelectron yield—in contrast to the spectral one [13]—requires the knowledge of both $\mathbf{B}$ and $\mathbf{T}$. Taking into account that the relevant B- and T-amplitudes are proportional to back-scattering ($\sim\int W(r)\exp(-2\mathrm{i}kr)\ \mathrm{d}r$) and forward-scattering ($\sim\int W(r)\ \mathrm{d}r$) form factors respectively, the reflectivity is less sensitive to the deformations of atomic potentials on the periphery due to atom–atom interaction in a chemical compound.

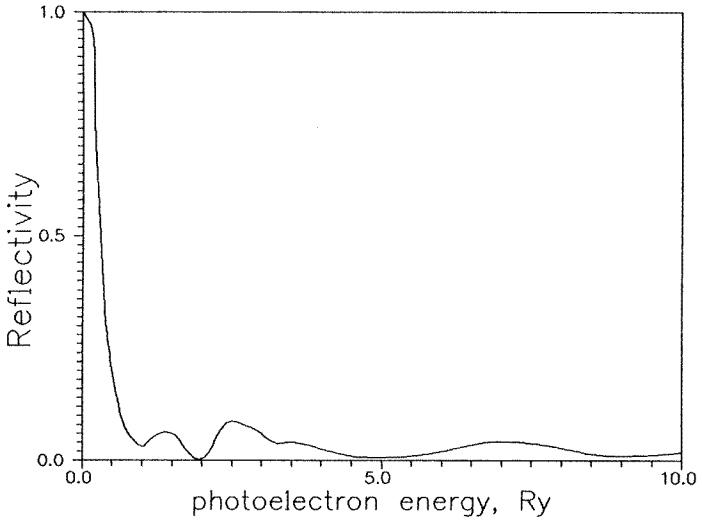

Figure 2. The spectral dependence of the reflectivity of the surroundings for photoelectrons ejected from the K shell of an Na^+ ion in NaF crystal [21].

The reflectivity $\mathcal{R}$ and transmission $\mathcal{T}$ of the surroundings are defined as

$$\mathcal{R}(E) = |B(E, b)|^2 \qquad \mathcal{T}(E) = |T(E, R)|^2. \tag{6}$$

Evidently, without inelastic losses [13]

$$\mathcal{R}(E) + \mathcal{T}(E) = 1. \tag{7}$$

For low E the reflectivity of the surroundings is high and the resonant $(\mathbf{1} - \mathbf{BS})^{-1}$-factor in equation (1) plays an important role. Moreover, as is seen from equations (2) and (3), $\mathcal{T}(E)$ can be found only if the reflection amplitudes are already known. In figure 2, the calculated spectral behaviour of the photoelectron reflectivity for NaF crystal [21] is shown, as an example. With E rising, $\mathcal{R}$ quickly drops and for $E > 30$ (or 50) eV (i.e. for the EXAFS region) the influence of $\mathbf{B}$ on J can be omitted. Then, for medium and high E equations (1) and (3) can be rewritten in a simpler form:

$$\varphi_g(E, \boldsymbol{r}) \approx \frac{1}{r}\sum_{l'\Gamma} T_{ll'\Gamma}(k)\exp\left[\mathrm{i}\left(kr - \frac{l'\pi}{2}\right)\right] Y_{l'\Gamma}(\Omega) \tag{8}$$

and

$$\frac{\mathrm{d}\mathbf{T}}{\mathrm{d}r} = -\mathbf{\Phi}^{-}\mathcal{W}\mathbf{\Phi}^{+}\mathbf{T} \tag{9}$$

showing that the single transmission dominates the anisotropy of the photoelectron yield. Formally the solution of equation (9) can be written as

$$\mathbf{T} = \exp\left(-\int_{surr} \mathbf{\Phi}^{-}\mathcal{W}\mathbf{\Phi}^{+}\,\mathrm{d}r\right) \tag{10}$$

which highlights the relationship between the transmission and the refraction of photoelectrons in the surroundings. In particular, for isotropic surroundings W_0 (i.e. without hybridization), replacing the $\mathbf{\Phi}^{\pm}$-functions by their asymptotes for the radial function (8) we have

$$\begin{aligned}\varphi_{gl}(r) &= \frac{1}{r}(2l+1)a_l(k)\exp\left[\mathrm{i}\left(kr-\frac{l\pi}{2}\right)\right]\exp\left[\frac{1}{2\mathrm{i}k}\int_0^r \exp\left[-\mathrm{i}\left(kr'-\frac{l\pi}{2}\right)\right]\right.\\ &\quad\left.\times W_0(r')\exp\left[\mathrm{i}\left(kr'-\frac{l\pi}{2}\right)\right]\mathrm{d}r'\right]\\ &= \frac{1}{r}(2l+1)a_l(k)\exp\left[\mathrm{i}\left(\frac{kr}{n(k)}-\frac{l\pi}{2}\right)\right]\end{aligned} \tag{11}$$

where

$$n(k) = 1 + \frac{1}{2k^2}\overline{W_0} \tag{12}$$

is a local refraction index for photoelectron waves in the surroundings and $a_l(k)$ is an amplitude of the atomic [core^{-1}kl] photoionization. The $n(k)$-definition (12) agrees with that obtained in [13, 22] where the solution of equation (2) was used to describe the spectral dependence of x-ray absorption far from the edges (the EXAFS region). In fact, for large r the values of $n(k)$ and $n(k,r)$ [13] coincide. Corresponding to the deceleration or acceleration of photoelectrons by the potential of the surroundings, the refractive index will be less or more than one. The substitution of k for k/n provides an effective way [13] of taking into account the contributions of numerous forward-scatterings occurring while photoelectrons are moving from an emitter to a detector. Since the potential of the surroundings averaged over the R_g-sphere, $\overline{W_0}$, is dependent on E, the dispersion of the photoelectron waves in the surroundings can depart from the normal law.

The photoelectron energy losses in the surroundings can be taken into account by adding an imaginary part to the $\mathcal{W}$-potential. For high and medium E the solution of equation (9) with the complex $\mathcal{W}$-potential (or optical potential) leads to a complex $n(k)$-index and, therefore, to an exponentially decreasing factor $\exp(-\overline{W_0}r/k^2)$ [13] in the expression for J. However, for low E, due to the dependence of $\mathbf{B}$ on the resonance, the photoelectron energy-loss effect on the diffraction pattern cannot be described by introducing this factor, and the exact solution of both (2) and (3) is required.

3. Model calculations

The above-described QA equations are now applied to calculate the angular distributions of photoelectrons emitted from K and $L_{2,3}$ inner shells of an atom (A) incorporated in octahedral [AX_6] clusters. We consider below the angular distributions of photoelectrons ejected from a 2p subshell of a Si atom in an $[SiF_6]^{2-}$ cluster with energies of 6 and 18 eV (subsection 3.1) and from K shells of Na^+ and F^- ions in various model [$A^{\pm}X_6$] clusters with $E \sim 40$ eV (subsection 3.2). These chosen cases allow one to examine, in an approximate fashion, the splitting and hybridization effects on the $J(\Omega)$-dependences separately.

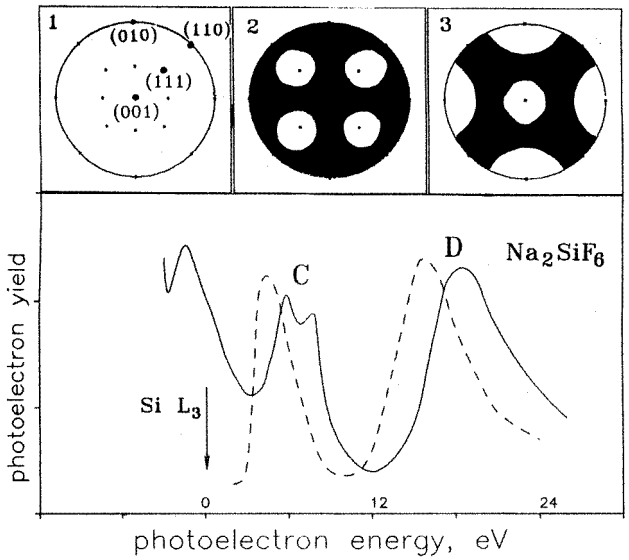

Figure 3. Upper panels: the stereographic projections of the main directions in an $[AX_6]$ cluster (1), and the angular distributions of photoelectrons ejected from the Si 2p subshell in a $[SiF_6]^{2-}$ cluster for $E = 6$ eV (2), and for $E = 18$ eV (3). Bottom: the spectral dependence of the photoabsorption cross section near the Si 2p edge in a Na_2SiF_6 crystal; experiment [23]—the solid line; calculations [13]—the dotted line.

In figure 3 the positions of the main (100), (111) and (110) axes in cubic clusters are marked in 2π-map 1. Because only one coordination shell surrounds an ionized atom (the source of outgoing electronic waves) the (100) directions correspond to the positions of the X atoms and (110), (111) ones can be formally attributed to 'virtual close-packed' directions in the cubic environment which are empty for the cluster approximation.

The QA approach was not applied here for the description of high-energy photoelectron diffraction due to difficulties arising (i) in the determination of the relevant $W(E, \boldsymbol{r})$-pseudopotential and (ii) in the growth of the ranges of the matrices **B** and **T**. Besides this, the influence of photoelectron flux dissipation in the surroundings on the diffraction patterns is ignored.

3.1. The splitting effect

Since the angular parts of various splitting components $\Gamma'(l)$ and $\Gamma''(l)$ are different, the low-energy photoelectron yield is anisotropic. To illustrate this effect the stereographic projections of the photoelectron yield from the 2p subshell of a silicon atom in an octahedral environment ($[SiF_6]^{2-}$) were computed with the help of equations (1)–(3) and the energy-dependent local pseudopotential of the surroundings. The projections found for outgoing electrons with kinetic energies $E \sim 6$ and 18 eV are plotted in figure 3 (maps 2 and 3 respectively). In order to simplify our calculations, the weak mixing of the dipole-allowed E s and E d partial waves in a_{1g}, e_g and t_{2g} channels with other l'-waves is not taken into account. The 2π-maps presented display primarily the angular distributions of the E d electrons, as their intensities are about one degree higher than that obtained for the E s electrons.

The stereographic projections in figure 3 clearly show the strong energy dependence. The intense $J(\Omega)$-maxima for $E = 6$ eV coincide with (111) directions; hence the photoelectrons go out of the compound between fluorine atoms, i.e. along threefold rotation axes, while for $E = 18$ eV they go out along (100) directions into the F atoms. These dramatic changes of the angular distributions occur for weak energy variations and have a resonance origin. According to our calculations it is the fact that the $[(\mathbf{1} - \mathbf{BS})^{-1}]_{22\Gamma}$ resonance factor is different for $\Gamma = \mathrm{e}_g$ and $\Gamma = \mathrm{t}_{2g}$ that leads to these features, and the photoelectron transmission effect on the patterns is weak.

The bright maxima in the two 2π-maps are connected with atomic Si $2\mathrm{p}^{-1}$ E d shape resonances split into doubly degenerate e_g and triply degenerate t_{2g} components. In our calculations the E-values are chosen with respect of the energy positions of the corresponding resonance features of x-ray absorption near the Si 2p edge in Na_2SiF_6 crystal. In figure 3 (bottom) the experimental [23] and the calculated QA absorption spectra [13] are plotted. The observed difference between the measured and computed resonance positions may be connected primarily with the single-electron approximation. At present the C and D resonances can be unambiguously assigned to transitions to these molecular states. The angular distributions 2 and 3 refer to the electron yield in resonant photoionization (resonances C and D in figure 3, respectively).

Analysing these patterns, we see that in the case of resonant photoemission the splitting of highly excited atomic resonances in polyatomic compounds leads to the appearance of strong angular and spectral dependences of the photoelectron yield. The maxima of the yield do not necessarily indicate the directions to the nearest neighbours, but coincide with the high-symmetry directions of the surroundings. This means that (i) the anisotropy of the photoelectron yield is induced by the *collective* action of all of the atoms in the environment and (ii) there is a strong correlation between low-energy photoelectron angular distributions and the symmetry of excited surface *molecular orbitals* (MOs) (or shape resonances) in agreement with the well-known assignment [24, 25] of resonance features in x-ray absorption/ionization spectra to transitions from inner-shell to excited MOs. Generalizing these results, we have to conclude that various polyatomic groups having the same symmetry point group cannot be unambiguously distinguished by examining a single low-energy diffraction pattern without making additional assumptions regarding their electronic structure. Hence, it is chemical rather than structural information on a specimen that can be extracted from a low-energy diffraction pattern analysis.

3.2. The hybridization effect

The effect of hybridization on atomic orbitals and its role in the formation of localized chemical bonds in chemical compounds is studied by considering the reduction of the total energy of their ground state (see, e.g., [26]). However, for highly excited states this effect remains obscure. To consider it, QA calculations of the angular distribution of K-shell photoemission from the central atom in various model octahedral $[AX_6]$ clusters are performed. Since the triply degenerate A 1s $(\mathrm{a}_{1g}) \rightarrow$ E $\mathrm{p}_{x,y,z}$ (t_{1u}) transitions are not split by the octahedral field, the pl'-hybridization is a single effect giving rise to anisotropy of the K-shell emission. To simplify our calculations we have considered the angular distribution of photoelectrons with kinetic energies equal to 40 eV for which the resonant factor $(\mathbf{1}-\mathbf{BS})^{-1}$ can be neglected and the number of l'-partial waves, rising with E, is not very high.

Because of this, only the first angle-dependent term with $\mu = 4$ in the multipole series (5) is taken into account. The series describes the interaction the $\mathrm{p}_{x,y,z}$ waves with l'-harmonics (where $|1 - \mu| \leqslant l' \leqslant |1 + \mu|$) in the dipole-allowed t_{1u} channel, which can be attributed

to the angular deformations of atomic photoelectron paths (or angular distributions) and to the pf and pfh hybridization of continuous partial atomic (A) states in the compounds. The inclusion of the following W_6-, W_8-, ..., W_{2n}-terms in the sum (5) is required to take into consideration the hybridization with higher l'-harmonics.

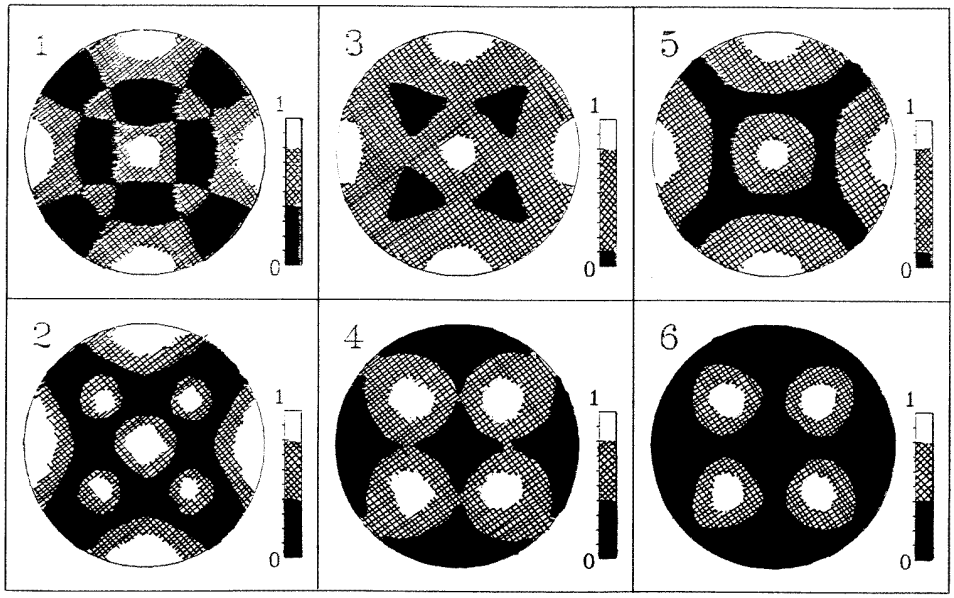

Figure 4. The stereographic projections of the cubic harmonics $f_{t_{1u}}$ (1) and $h_{t_{1u}}$ (2), and of the photoelectron yield ($E = 40$ eV) from the K shell of central ions in $[Na^+F_6^-]$ (3) and $[F^-Na_6^+]$ (4) with the pf hybridization in the same clusters as the pfh hybridization, (5) and (6) respectively.

The stereographic projections computed taking account of the pf and pfh hybridizations, using equations (8) and (9), are plotted in figure 4 (maps 3–6). As can be seen, the pf hybridization strongly deforms the initially isotropic E p photoelectron flux, focusing it along various Ω_S-directions. The Ω_S-sets found characterize the symmetry $\mathcal{G}$ of an ionized atom in the compounds coinciding with the fourfold and threefold rotation axes rather than the directions along the A–X chains. To clarify the observed relationship between the hybridization and crystallographic effects, the angular distributions of (O_h) symmetry-adapted $f_{t_{1u}}$ and $h_{t_{1u}}$ harmonics are shown in figure 4, maps 1 and 2. They demonstrate the correlation of the positions of their maxima, minima and saddle points with the main crystallographic axes. Hence, from the QA viewpoint, the (100), (110) and (111) directions become selected due to the hybridization of the isotropic p waves with the higher harmonics in the t_{1u} channel.

The $W(E, r)$-value, due to its pseudopotential nature, varies dramatically according to the type of the environment atoms (primarily as regards the energy position of the upper occupied orbitals [27]) and their chemical state. In order to illustrate the influence on photoelectron diffraction, the 2π-maps computed for one cluster geometry and kinetic photoelectron energy but for different potentials of the surroundings are shown in figure 4. Maps 3 and 4 can be attributed to the K-shell photoemission from central ions in $[Na^+F_6^-]$ and $[F^-Na_6^+]$ clusters in a NaF crystal, respectively, with account taken of the pf

hybridization. A strong chemical effect on the photoelectron angular distributions is clearly seen. In fact the electronic charge transfer controls the brightness along the main (100) and (111) directions in the crystal. The intensity of the photoelectron flux along (111) directions opposite to (100) ones increases with the reduction of electronegativity of the nearest neighbours. As a result, the angular dependences found for the K-shell emission from anions and cations in the crystal differ so strongly that map 3 looks almost like the negative of map 4 in figure 4.

For general reasons, the contribution of higher l-harmonics growing with E to the diffraction pattern has to change the intensities along the main directions and generate the appearance of additional extremes of photoelectron yield. Maps 5 and 6 in figure 4 demonstrate the angular distributions of photoelectrons from the $[Na^+F_6^-]$ and $[F^-Na_6^+]$ clusters found taking into account pfh hybridization. Comparison of maps 3 and 4 with maps 5 and 6 shows that the inclusion of the h waves noticeably affects the intensities, but new selected directions of photoelectron yield do not appear. However, according to our preliminary calculations, they do appear if the $l' = 7$ harmonics are included.

4. Discussion and conclusions

Summarizing the results from the application of the QA approach to inner-shell photoionization in the octahedral clusters, we conclude that angular distributions of low- and medium-energy photoelectrons can be regarded and described as reflecting the impact of the surroundings on the atomic photoelectron flux. The analysis of our $J(\Omega)$-calculations provides evidence of the following.

(i) The appearance of strong anisotropy in the photoelectron yield due to the splitting of degenerate atomic-core–continuum transitions and the hybridization of atomic continuous states with different angular momenta.

(ii) The central role of the collective effect of all of the environment atoms, whose symmetry compels the major directions of photoelectron yield to coincide with the main crystallographic axes but not necessarily with the directions to the nearest neighbours (i.e. unlike in the case of high-energy photoelectron diffraction).

(iii) The high sensitivity of low- and medium-energy diffraction patterns to the electronic structure of the ionized atom and the integral electron-optical properties of the surroundings.

(iv) The dramatic changes in the angular distribution of photoelectrons when resonant inner-shell photoemission occurs.

As a result, the possibilities (i) of rationalizing low- and medium-energy photoelectron angular distributions from quantum chemical positions and (ii) of considering the diffraction patterns as a source of additional information on chemical bonding and angular deformations of electron density distributions in atoms on surfaces arise. While the atomic deformations can be described on the basis of crystallographic positions, their quantitative values are determined primarily by the atom–atom interaction responsible for chemical bonding.

From the QA point of view, the splitting of an atomic Si $2p^{-1}$ E d shape resonance dominates the angular dependence of resonant photoelectron emission from the the Si 2p subshell in the $[SiF_6]^{2-}$ cluster. Comparison of this with the Si $L_{2,3}$ XANES of Na_2SiF_6 crystal [23] makes clear (i) the essentially resonance origin of the $J(\Omega)$-dependence which changes quickly with weak variations of photoelectron kinetic energies from 6 eV to 18 eV and (ii) the strong correlation of the angular distribution with the symmetry of the related highly unoccupied E e_g and E t_{2g} MOs. In its turn, the hybridization of atomic continuum states dominates the anisotropy of the photoelectron emission from the K shell in the

octahedral clusters. The calculations of transitions from the 1s (a_{1g}) level to dipole-allowed continuous E t_{1u} states (for $E = 40$ eV, i.e. outside the XANES region) with account taken of the pf and pfh hybridization have demonstrated the strong angular dependence of the photoelectron distribution and its sensitivity to the atomic composition of the surroundings.

The hybridization effect can be attributed to the angular deformations of electron paths by impacts from the surroundings and regarded as being responsible for the focusing/defocusing of electron waves along various directions. This focusing effect can be explained by means of the photoelectron refraction of the surroundings, allowing us to connect in a simple way the formation mechanisms of photoelectron diffraction patterns for high- and medium-energy regimes. (For low E the refraction cannot be used to provide a satisfactory description, as the resonance effect caused by high reflectivity of the surroundings must be taken into consideration.) In all of the cases under study the calculated $J(\Omega)$-maxima of the K-shell emission can be assigned to the directions in the surroundings with maximal electron-optical density, not necessarily coinciding with A–X chains.

As the chemical effects decrease in strength with increase of E, it is the distribution of atomic cores that dominates the anisotropy of the electron-optical properties of the surroundings. As a result, the close resemblance of the effects of refraction and forward-scattering along close-packing directions on the high-energy photoelectron diffraction arises. Since the anisotropy and the focusing properties of the surroundings become less pronounced with the growth of the distance from the ionized-core atom, the focusing of photoelectron waves along long atomic chains in crystals is impossible. The differences between the refraction and forward-scattering effects becomes most evident on comparison of photoemission from anions and cations in a NaF crystal for medium energy. The relevant stereograph projections for $E = 40$ eV (figure 4) with refraction taken into account look like negatives, whereas using the forward-scattering mechanism the expected projections will be practically indistinguishable. Hence (1) the collective action of neighbours determines the angular distributions and (2) clusters having the same symmetry (e.g. $[AX_6]$, $[AX_8]$, $[AX_6Y_8]$, $[AX_6Y_{12}Z_8]$, ...) cannot be unambiguously distinguished on the basis of just the analysis of a single low-energy diffraction pattern without making additional assumptions regarding the cluster electronic structure.

The angular distributions in figure 3 and 4 were computed with the application of the different sets of equations (1)–(3) and (8), (9) respectively. Both sets describe the collective effect of the environment subsystem on ionized-core atoms. For low E, when equations (1)–(3) are used, the contributions of multicentre paths such as $Si \rightarrow F_1 \rightarrow Si \rightarrow F_2 \cdots$ and the angular deformations of the atomic electron density in compounds dominate this effect. But for medium E the atomic density angular deformations are the single cause responsible for the collective action, as equations (8) and (9) take into account forward-scattering effects only and the contributions of the multicentre paths in the small clusters under study disappear. These deformations are closely connected with chemical bonding and, in particular, with electronic charge transfer which characterizes the quantitative value of multipole momenta W_μ and, therefore, the focusing properties of the surroundings. This relationship between the charge transfer and hybridization was used in [28] to reveal the effect of hybridization on the x-ray absorption near-edge structure and to rationalize the spectral dependence of S K-shell absorption in thiophene and related compounds.

The angular distribution of low-energy photoelectrons (or Auger electrons) scattered from surfaces can be noticeably modified by the surface dipole momentum $\boldsymbol{d}_s$. In particular, the spdf... hybridization will be allowed for the octahedral clusters due to their weak deformations in the surface region. One would expect that on analysing the multipole

expansion found with the help of relevant experimental data, it would be found that information about the d_s-value could be extracted.

References

[1] 1993 *Materials Workshop on Photoelectron Diffraction (Gwatt, Switzerland)*
[2] Fadley C S 1990 *Synchrotron Radiation Research: Advances in Surface Science* ch 11 (New York: Plenum); 1987 *Phys. Scr.* **17** 39
[3] Chambers S A 1991 *Adv. Phys.* **40** 357
[4] Chambers S A 1992 *Surf. Sci. Rep.* **16** 261
[5] Fadley C S 1993 *Surf. Sci. Rep.* **19** 231
[6] Davis R, Woodruff D P, Xu X M, Weiss K U, Dippel R, Schindler K M, Hoffmann P, Fritzsche V and Bradschaw A M 1994 *14th Europ. Conf. on Surf. Sci. (Leipzig)* abstracts, p 221
[7] Greber T, Osterwalder J, Naumovic D, Stuck A, Hufner S and Schlapbach 1992 *Phys. Rev. Lett.* **69** 1947
[8] Greber T, Osterwalder J, Hufner S and Schlapbach 1992 *Phys. Rev.* B **45** 4540
[9] Fritzsche V 1990 *J. Phys.: Condens. Matter* **2** 9735
[10] Fritzsche V and Pendry J B 1993 *Phys. Rev.* B **48** 9054
[11] Mustre de Leon J, Rehr J J, Natoli C R, Fadley C S and Osterwalder J 1989 *Phys. Rev.* B **39** 5632
[12] Ziman J M 1972 *Principles of the Theory of Solids* (Cambridge: Cambridge University Press)
[13] Pavlychev A A, Vinogradov A S, Stepanov A P and Shulakov A S 1993 *Opt. Spectrosc.* **75** 554
[14] Hallmeier K H, Pavlychev A A, Szargan R, Beyer L, Hennig C and Thiel F 1993 *Chem. Phys.* **178** 349
[15] Pavlychev A A, Vinogradov A S, Akimov V N and Nekipelov S V 1990 *Phys. Scr.* **41** 160
[16] Adams W H 1962 *J. Chem. Phys.* **37** 2009
[17] Gilbert T L 1964 *Molecular Orbitals in Chemistry, Physics and Biology* (New York) p 405
[18] Babikov V V 1976 *Variable Phase Approach in Quantum Mechnics* (Moscow: Nauka) (in Russian)
[19] Calogero F 1967 *Variable Phase Approach to Potential Scattering* (New York: Academic)
[20] McWeeny R 1963 *Symmetry* (Oxford: Pergamon)
[21] Kondratieva I V 1987 *Thesis Doc. Diss.* Leningrad State University
[22] Pavlychev A A, Vinogradov A S and Kondratieva I V 1986 *Sov. J. Solid State Phys.* **28** 837
[23] Fomichev V A and Nefedov V I 1968 *J. Struct. Chem. (URSS)* **9** 279
[24] Gianturco F A, Guidotti M and Lamanna M 1992 *J. Chem. Phys.* **57** 840
[25] Pavlychev A A, Hitchcock A P, Reynaud C, Bodeur S and Nenner I 1996 *Chem. Phys.* at press
[26] Magnusson E 1990 *J. Am. Chem. Soc.* **112** 7940
[27] Demkov Yu N and Ostrovsky V N 1971 *The Zero Range Potential Method in Atomic Physics* (Leningrad: LGU) (in Russian)
[28] Pavlychev A A, Fominykh N G, Winter I and Hormes J 1996 *11th Int. Conf on VUV Physics (Tokyo, 1995); J. Electron Spectrosc. Relat. Phenom.* at press